International Journal of Control, Automation, and Systems 22(1) (2024) 1-15
http://dx.doi.org/10.1007/s12555-023-0132-1
ISSN:1598-6446 eISSN:2005-4092
http://www.springer.com/12555

Coordination of Active Front Steering and Direct Yaw Control Systems Using MIMO Sliding Mode Control

Ebrahim Muhammad, Ahmad Reza Vali, Abdorreza Kashaninia, and Vahid Behnamgol*

Abstract: This paper investigates an integrated multi-input multi-output (MIMO) sliding mode control strategy to coordinate the active front steering (AFS) and direct yaw control (DYC) system of a vehicle. The proposed control method aims to enhance the lateral dynamics of the vehicle, especially in the presence of tire-road friction coefficient variations as parameter uncertainties. The proposed integrated control strategy consists of two control layers. The upper layer coordinates the AFS and DYC systems and produces the corrective yaw moment and additive front steering angle. At the lower layer, the slip controller based on sliding mode control (SMC) converts the yaw moment into the desired longitudinal slip and generates the final distributed braking torques. Simulations of two scenarios in various road conditions were conducted to ensure that the proposed control is robust against road condition changes in the proposed method. Results from the simulation during the J-turn maneuver on the slippery road compared the performance of the suggested sliding mode integrated controller with an adaptive integrated controller. The simulation results showed that the proposed control system improved the stability and handling of the system's tracking performance in various maneuvers.

Keywords: Active front control, direct yaw moment control, integrated control, lateral vehicle stability, sliding mode control.

1. INTRODUCTION

Direct yaw control is a central component of active chassis control, which improves vehicle stability without sacrificing performance and reduces accidents caused by loss of stability. The active front steering (AFS) and direct yaw control (DYC) systems participate in yaw moment control according to specific tire working areas. AFS focuses on steering angle compensation via the active steering actuator, making it an indirect yaw moment control system. At the same time, in the DYC system, the differential brake system provides different brake forces to the two sides of the vehicle to interfere directly with yaw motions [1,2]. AFS steering compensation is adequate to control the vehicle's yaw moment in the linear region of tire work without activating the DYC. This enhances lateral stability and controllability and eliminates the driver-inconvenient effect of the DYC system intervention on the longitudinal vehicle dynamics. While AFS becomes less effective in the nonlinear region of tire working where the tire lateral forces saturate, the DYC system is activated in these situations [3]. An integrated control strategy is utilized to enhance vehicle stability and safety [4] because of the two systems' distinct working areas and coupling effects. There are several ways to coordinate the AFS and DYC systems [5,6]. Some researchers in many recent studies have used the phase plane of sideslip angle and its time derivative to switch between AFS and DYC according to the region of tire work [7,8].

Many control strategies for integrated control of AFS and DYC systems have been presented in the literature. In [9], Jalali *et al*. designed an MPC controller for coordinating the AFS and DYC systems to improve lateral stability. In [10], Doumiati *et al*. introduced a multi-variable control system based on H_∞ for integrating AFS and DYC to improve vehicle handling and stability by tracking the required yaw rate and minimizing the use of brake actuators. The control system in the higher layer generates the compensatory yaw moment required for integration with the active front steering system. The torque difference between the vehicle's two sides can produce the desired yaw moment command. In [11], Mirzaei and Mirzaeinejad designed an optimal multivariable controller to integrate AFS and DYC using the prediction of nonlinear responses of an 8-DOF vehicle model. In order to achieve directional stability, the AFS is integrated with the braking system to reduce the maximum braking force of traditional Anti-lock braking systems (ABS), allowing the shortest

Manuscript received February 24, 2023; revised July 3, 2023; accepted August 20, 2023. Recommended by Associate Editor Seung Jae Lee under the direction of Senior Editor Jongeun Choi.

Ebrahim Muhammad, Ahmad Reza Vali, Abdorreza Kashaninia, and Vahid Behnamgol are with the School of Electrical and Computer Engineering, Malek Ashter University of Technology, Tehran, Iran (e-mails: ebramm100@gmail.com, {vali, akashaninia, vahid_behnamgol}@mut.ac.ir).
* Corresponding author.

braking distance while maintaining directional stability. In [12], Ahmadian *et al*. developed a hierarchical integrated control strategy to coordinate AFS and DYC, enhancing the performance of yaw rate tracking control and limiting sideslip angle. The proposed control structure has two levels. Through MIMO adaptive laws, an indirect adaptive control method was developed at the upper control level to design an additive steering angle and corrective yaw moment. An optimization algorithm was used at the lower control level to distribute the brake forces to the rear wheels and convert the external yaw moment into brake torques. In [13], Ding and Taheri proposed an adaptive controller based on the direct Lyapunov method to integrate the AFS and DYC systems, including the diversity of corning stiffness during adaption laws, to ensure vehicle stability in critical conditions. In [14], Zhang *et al*. presented a robust adaptive controller with an uncertainty observer to integrate AFS and DYC systems via Lyapunov stability theory to calculate the corrective yaw moment. The system was modeled as an integrated chassis control model containing multiplicative uncertainties. An adaptive law has been designed based on the projection correction method to estimate and compensate for those uncertainties.

The sliding mode control (SMC) strategy for vehicle stability control has been studied extensively. In [15], Mashadi and Majidi developed a multi-layer sliding mode controller to integrate the AFS and DYC systems by combining vehicle yaw rate and lateral slip angle errors in a sliding surface equation to obtain the corrective steering angle and yaw moment in the upper layer to generate the final braking torque using two electric motors planted in the rear wheels. In [16], Saikia and Mahanta developed a sliding mode controller based on the PID controller considering only the yaw rate as a control variable on the sliding mode surface. That enhanced the vehicle's transient performance by integrating active front steering and direct yaw moment into two control layers. The vehicle's yaw rate and side slip angle are tracked, enhancing handling performance. The corrective front steering and the external yaw moment are generated in the upper layer. The latter input control is used through differential braking in the lower layer. In [17], Feng *et al*. proposed a three-layer hierarchical approach for improving the stability of vehicles when driving through corners by employing four-wheel differential braking, four-wheel drive, and active front steering. Based on the sliding mode control theory, the upper-level control tracks the desired vehicle motion by calculating the desired yaw moment and longitudinal forces based on two independent sliding surfaces. An optimal control method distributes operator commands at the lower layer. In [18], Liu *et al*. present a super-twist algorithm sliding mode control for coordinating AFS and DYC systems using a linear sliding surface combining the normalized absolute values of yaw rate error and sideslip error to improve path-following accuracy and ensure vehicle stability. This control method reduced the lateral offset and head angle deviation as much as possible and avoided the chatter phenomenon of traditional sliding mode control. In [19], Zhang and Li presented a hierarchical control strategy based on the fast terminal sliding mode control (FTSMC) method of AFS and DYC coordination based on a combination of vehicle yaw rate and lateral slip angle errors in a sliding surface to improve vehicle stability. In addition to calculating the corrective yaw moments at the upper level of control, the lower level of control converts them into the required longitudinal slips. This control strategy increased the front wheels' steering angle according to each wheel actuator's limitations.

Based on the literature review, which showed different applications of the integration of active front steering and direct yaw moment for vehicle stability control, no studies based on the MIMO sliding mode control (MSMC) method were found to enhance vehicle stability and handling. Therefore, this paper aims to use the MIMO sliding mode control (MSMC) method to coordinate the AFS and DYC to enhance vehicle stability and handling in the presence of uncertainties.

In this paper, an integrated strategy of active front steering and direct yaw moment in a hierarchical manner based on the MIMO sliding mode control (MSMC) method is proposed for the first time to enhance vehicle stability and handling. The proposed strategy consists of two levels of control. The main objective of the upper layer is to generate a robust and accurate external yaw moment by controlling both the braking forces on the two sides of the vehicle and the corrective front steering angle based on the proposed novel sliding mode controller. The stability index illustrates the combination of AFC and DYC based on the phase plane of the sideslip and its time derivative. As a part of the lower layer, a slip controller based on SMC converts the yaw moment into the longitudinal slip and then generates the final distributed braking torques.

The main contribution of this study is the following:

1) Various studies applying SMC have been conducted. However, no studies have been found to integrate the AFS and DYC systems using MSMC to enhance vehicle stability and handling in the presence of uncertainties by maintaining the sideslip angle at a smaller value than required while tracking the desired yaw rate.
2) Tire forces do not occur instantly due to a specific slip ratio but take time to build up when a force is applied to a tire. At high speeds and critical maneuvers, such as avoiding obstacles or hard braking, delays in transmitting forces to the tires can result in losing control of the vehicle. While most control research ignores this delay for simplification, this paper uses a typical dynamical model to express this delay by applying a

first-order delay to the lateral forces.

3) Most previous studies considered parametric uncertainties in vehicle parameters such as total mass, moment of inertia and tire stiffness. Whereas this research includes the road tire friction coefficient along with these parameters in the vehicle model as uncertainties to evaluate the performance of the MSMC in improving vehicle stability in the presence of uncertainties.
4) Proving the stability of a closed-loop control system incorporating the model, controller and observer estimating the sideslip angle and tire forces in the presence of uncertainties.

The rest of this paper is organized as follows: Section 2 describes the vehicle dynamics model. Section 3 presents the MSMC based on a hierarchical control structure. Section 4 discusses the simulation results and discussion. Finally, Section 5 presents the conclusion.

2. VEHICLE DYNAMICS MODEL

This section uses two different vehicle models: a non-linear 8-DOF vehicle model for designing the integrated MSMC and for results' simulation, and a 2-DOF model to generate the desired yaw rate and sideslip angle.

2.1. 8-DOF vehicle model

Fig. 1 shows the general layout of a non-linear 8-DOF vehicle model that includes the longitudinal velocity v_x, the lateral velocity v_y, the yaw rate r, the roll rate p, and the rotational speed of each wheel (ω_{fR}, ω_{fL}, ω_{rR}, ω_{rL}) that can be modeled based on Fig. 2.

According to Fig. 1, the governing equations for a vehicle body motion can be described as follows [12,20]:

$$m\dot{v}_x = mv_y r + F_{xfR} + F_{xfL} + F_{xrR} + F_{xrL} - F_{aero}, \quad (1)$$

$$m\dot{v}_y = -mv_x r - m_s h_s \dot{p} + F_{yfR} + F_{yfL} + F_{yrR} + F_{yrL}, \quad (2)$$

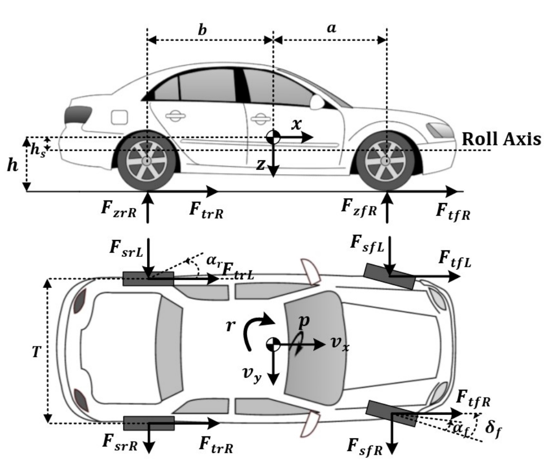

Fig. 1. 8-DoF vehicle dynamics model.

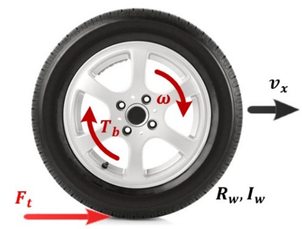

Fig. 2. Free diagram of the wheel.

Table 1. Vehicle parameters [12].

Parameter	Description	Amount
m	Total mass of the vehicle (kg)	1280
m_s	Sprung mass of the vehicle (kg)	1160
a	Distance from the vehicle's CG to the front axles (m)	1.203
b	Distance from the vehicle's CG to the rear axles (m)	1.217
T	Width of the track (m)	1.33
h	Height of the vehicle's center of gravity (m)	0.5
h_c	Distance from the sprung mass center of gravity to the roll axis (m)	0.2
I_{zz}	Yaw moment of inertia ($kg.m^2$)	2500
I_{xx_s}	Roll moment of inertia ($kg.m^2$)	750
I_{xz_s}	Product of inertia of roll and yaw axes ($kg.m^2$)	0
R_w	Wheel radius (m)	0.3
I_w	Wheel moment of inertia ($kg.m^2$)	2.1
C_α	Cornering tire stiffness (N/rad)	40000
C_λ	Longitudinal tire stiffness (N/unit slip)	50000
K_{RSF}	Ratio of front roll stiffness to the total stiffness (rad/rad)	0.444
K_{rsf}	Roll steer coefficient at the front (rad/rad)	-0.2
K_{rsr}	Roll steer coefficient at the rear (rad/rad)	0.2
$K_\emptyset$	Roll stiffness coefficient (Nm/rad)	45000
$C_\emptyset$	Roll stiffness damping (Nm/rad/sec)	2600
ε_r	Factor of road adhesion (s/m)	0.015
g	Gravitational acceleration (m/s^2)	9.81
C_d	Drag coefficient	0.3
ρ_a	Air density (Kg/m^3)	1.206
A_f	Frontal area (m^2)	2.51
RL_y	Tire relaxation length (m)	0.3

$$I_{zz}\dot{r} = I_{xz_s}\dot{p} + a(F_{yfR} + F_{yfL}) - b(F_{yrR} + F_{yrL}) + \frac{T}{2}[(F_{xfL} + F_{xrL}) - (F_{xfR} + F_{xrR})], \quad (3)$$

$$I_{xx_s}\dot{p} = -m_s h_s \dot{v}_y + I_{xz_s}\dot{r} - m_s h_s v_x r + m_s g h_s sin\emptyset - K_\emptyset \emptyset - C_\emptyset \dot{\emptyset}, \quad (4)$$

$$I_w \dot{\omega}_i = -R_w F_{ti} + T_{bi}, \text{ with } i = fL,\ fR,\ rL,\ rR, \quad (5)$$

$$\dot{\emptyset} = p. \quad (6)$$

Table 1 lists the parameters used in the simulation and equations for vehicle dynamics.

Also, $\emptyset$ is the roll angle of the vehicle, ω is the angular velocity of the wheels, and T_{bi} are four-wheel braking torques. F_{aero} indicates the aerodynamic drag forces as follows [12,21]:

$$F_{aero} = 0.5\rho_a C_d A_f v_x^2. \tag{7}$$

According to the vehicle's steer angle δ_i, the following equations transfer tire forces from the wheel-fixed coordinate system to the vehicle-fixed coordinate system

$$F_{xi} = F_{ti}\cos\delta_i - F_{si}\sin\delta_i, \text{ with } i = fL,\ fR,\ rL,\ rR, \tag{8}$$

$$F_{yi} = F_{ti}\sin\delta_i - F_{si}\cos\delta_i, \text{ with } i = fL,\ fR,\ rL,\ rR, \tag{9}$$

where F_x and F_y are the longitudinal and lateral forces of tires in the vehicle fixed, F_t and F_s are the traction forces and the lateral forces of the tire in the wheel fixed coordinate system, respectively. Small letters (f, r) indicate the position of the front and rear wheels, and capital letters (L, R) indicate the position of the left and right wheels.

Three assumptions [12,15,21] are made on the vehicle model.

Assumption 1: The moment of inertia for roll and yaw is neglected for simplicity.

Assumption 2: The steering angles δ_{rL} and δ_{rR} were considered to be equal to zero.

Assumption 3: The steering angles of the front and rear wheels are influenced by the rolling motion of the vehicle body due to the suspension kinematics

$$\delta_{fL} = \delta_{fR} = \delta_{sw} + K_{rsf}.\emptyset, \tag{10}$$

$$\delta_{rL} = \delta_{rR} = K_{rsr}.\emptyset, \tag{11}$$

where δ_{sw} is the steering angle of the hand wheel.

2.2. Tire model

Dugoff model was chosen to simulate the non-linear system of tires because the longitudinal and lateral forces of the tires are directly related to the road factor [22,23].

The following equations give the lateral and longitudinal forces according to Dugoff model

$$\begin{aligned} F_{si} &= \frac{C_\alpha tan(\alpha_i)}{1-\lambda_i} f(s_i),\ i = fL,\ fR,\ rL,\ rR, \\ F_{ti} &= \frac{C_\lambda \lambda_i}{1-\lambda_i} f(s_i),\ i = fL,\ fR,\ rL,\ rR, \end{aligned} \tag{12}$$

where

$$f(s_i) = \begin{cases} s_i(2-s_i), & s_i < 1, \\ 1, & s_i \geq 1, \end{cases} \quad i = fL,\ fR,\ rL,\ rR, \tag{13}$$

and

$$s_i = \frac{\mu F_{zi}(1-\varepsilon_r v_x\sqrt{\lambda_i^2 + tan^2(\alpha_i)})}{2\sqrt{C_\lambda^2\lambda_i^2 + C_\alpha^2 tan^2(\alpha_i)}}(1-\lambda_i),$$

$$i = fL,\ fR,\ rL,\ rR, \tag{14}$$

where μ is the tire-road friction coefficient.

λ_i and α_i are the tire-road longitudinal slip ratio and slip angle, respectively, given by the following relations [24]

$$\lambda_i = \begin{cases} -1 + \dfrac{R_w\omega_i}{v_{xwi}}, & R_w\omega_i < v_{xwi}, \\ 1 - \dfrac{v_{xwi}}{R_w\omega_i}, & R_w\omega_i \geq v_{xwi}, \end{cases} \tag{15}$$

with $i = fL, fR, rL, rR$,

$$\begin{aligned} \alpha_{fL} &= \delta_{fL} - \tan^{-1}((v_y + ar)/(v_x + 0.5Tr)), \\ \alpha_{fR} &= \delta_{fR} - \tan^{-1}((v_y + ar)/(v_x - 0.5Tr)), \\ \alpha_{rL} &= \delta_{rL} + \tan^{-1}((br - v_y)/(v_x + 0.5Tr)), \\ \alpha_{rR} &= \delta_{rR} + \tan^{-1}((br - v_y)/(v_x + 0.5Tr)). \end{aligned} \tag{16}$$

The following equations give the longitudinal velocity of the wheels' center

$$\begin{aligned} v_{xwfL} &= (v_x + 0.5Tr)\cos\delta_{fL} + (v_y + ar)\sin\delta_{fL}, \\ v_{xwfR} &= (v_x - 0.5Tr)\cos\delta_{fR} + (v_y + ar)\sin\delta_{fR}, \\ v_{xwrL} &= (v_x + 0.5Tr)\cos\delta_{rL} - (br - v_y)\sin\delta_{rL}, \\ v_{xwrR} &= (v_x - 0.5Tr)\cos\delta_{rR} - (br - v_y)\sin\delta_{rR}. \end{aligned} \tag{17}$$

F_z is the normal load of each tire given by the following equations

$$\begin{aligned} F_{zfL} &= \frac{mgb}{2l} - \frac{ma_xh}{2l} + K_{RSF}\left(\frac{ma_yh}{T} - \frac{m_sgh_s}{T}sin\emptyset\right), \\ F_{zfR} &= \frac{mgb}{2l} - \frac{ma_xh}{2l} - K_{RSF}\left(\frac{ma_yh}{T} - \frac{m_sgh_s}{T}sin\emptyset\right), \\ F_{zrL} &= \frac{mga}{2l} - \frac{ma_xh}{2l} \\ &\quad + (1-K_{RSF})\left(\frac{ma_yh}{T} - \frac{m_sgh_s}{T}\sin\emptyset\right), \\ F_{zrR} &= \frac{mga}{2l} - \frac{ma_xh}{2l} \\ &\quad - (1-K_{RSF})\left(\frac{ma_yh}{T} - \frac{m_sgh_s}{T}\sin\emptyset\right). \end{aligned} \tag{18}$$

Additionally, a_y represents the vehicle's lateral acceleration, while l represents the vehicle's longitudinal wheelbase. In addition, due to the significant effect of the tire force lag on the lateral vehicle dynamics in response to high-acceleration maneuvers, it was taken as a first-order delay [15,25]

$$\tau\dot{F}_s + F_s = F_{sss}. \tag{19}$$

The lateral tire force F_{sss} in the steady state during the time constant τ is given as

$$\tau = RL_y/u.$$

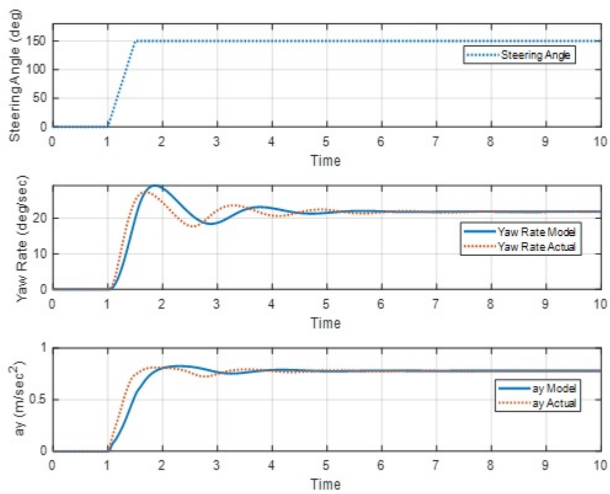

Fig. 3. The validation of the yaw rate response and lateral acceleration.

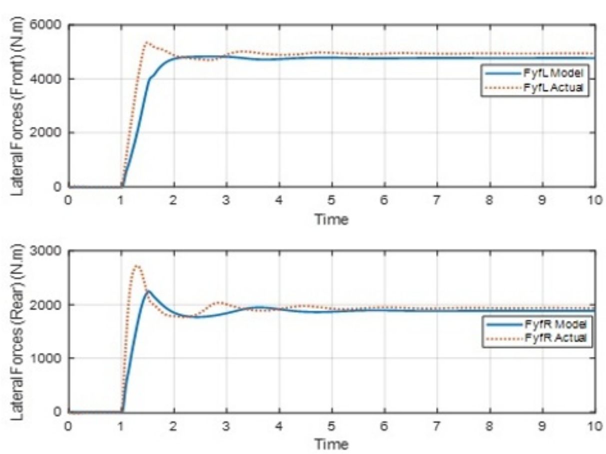

Fig. 4. The validation of the front and rear lateral forces.

One of the most critical steps in the simulation process is validating the mathematical model. At the end of this section, the nonlinear 8-DOF vehicle model was validated by comparing it to actual vehicle test data in the CARSEM program on the sedan D-Class. Fig. 3 compares the yaw rate response and lateral acceleration of a runaway vehicle on a dry road at a constant speed of 20 meters per second based on a J-turn maneuver with a steering wheel angle of 150 degrees. Fig. 4 compares the front and rear lateral forces resulting from the nonlinear 8-DOF vehicle model with the actual vehicle test data. This review suggests that the results of the vehicle's mathematical model match well with the actual measurements of the vehicle.

2.3. Reference model

The 2-DoF vehicle model is used in this paper to calculate yaw rate and sideslip angle references. Fig. 5 shows a 2-DOF vehicle model with lateral motions.

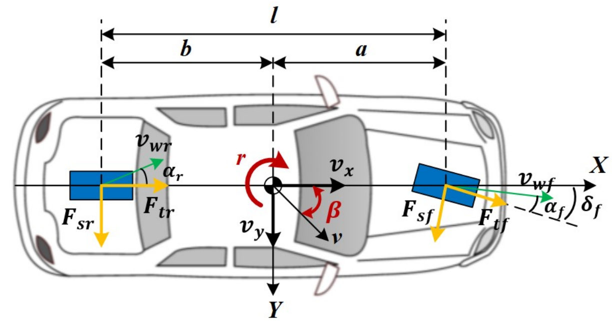

Fig. 5. Framework of linear 2-DOF vehicle model.

The following formulas can be used to determine the vehicle's desired yaw rate and sideslip angle [23,24]

$$r_{ss} = \frac{v_x}{l + K_{US} v_x^2}\delta_f, \tag{20}$$

$$\beta_{ss} = \frac{1}{l + K_{US} v_x^2}\left(b - \frac{a}{l}\frac{m}{2C_{\alpha r}}v_x^2\right)\delta_f. \tag{21}$$

KUS is called the vehicle's understeer coefficient. It is given by

$$K_{US} = \frac{m(bC_{\alpha r} - aC_{\alpha f})}{2lC_{\alpha f}C_{\alpha r}}. \tag{22}$$

It should be noted that the desired yaw rate and lateral slip angle cannot be achieved if the tire force exceeds the physical adhesion limit of the tire. Equations (23) and (24) provide upper limits for the desired yaw rate and lateral slip angle, respectively.

$$r_d = 0.85\frac{\mu g}{v_x}, \tag{23}$$

$$\beta_d = \arctan(0.02\mu g). \tag{24}$$

In this study, the MSMC is designed to track the desired yaw rate while maintaining a sideslip angle equal to or less than the desired value.

3. THE PROPOSED CONTROLLER DESIGN

The overall structure of the proposed integrated control system with two layers is shown in Fig. 6.

The proposed control system is composed of two layers. In the upper layer, the main objective is generating appropriate external yaw moment and corrective front steering angle based on the novel sliding mode controller. In the lower layer, the slip controller based on SMC is designed to trace the desired longitudinal slip converted from the yaw moment, then the final distributed braking torques on the rear wheels are generated.

3.1. High-level controller design

In this section, due to the nonlinearity of the vehicle and the uncertainty in its dynamics, the sliding mode control technique was used to ensure the vehicle's stability by

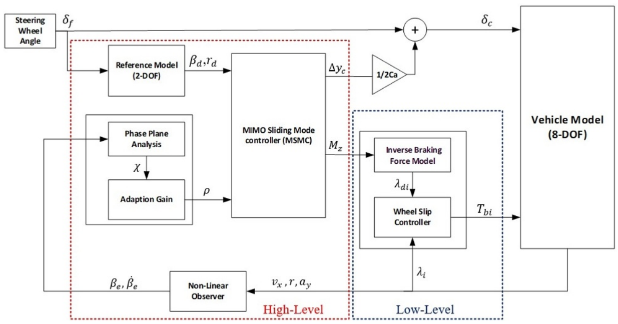

Fig. 6. Overall structure of the proposed integrated control system.

tracking the yaw rate and maintaining the slip angle in the stability zone. According to the desired yaw rate and side slip, a MIMO sliding mode controller (MSMC) with two sliding surfaces is designed to produce the external yaw moment and the wheel's corrective lateral force $(M_z, \Delta y_c)$ as two control inputs. Since the lateral slip angle cannot be measured directly, the side slip angle and its derivative $(\beta, \dot{\beta})$ are estimated by a nonlinear observer [26] to produce the stability index resulting from the Phase Plane Stability. Adaptive gain (ρ) determines the effect of both AFS and DYC control systems on the proposed final output of the integrated control system.

To design the upper layer controller, the output vector is $y = [y_1 \quad y_2]^T = [\beta \quad r]^T$, and the control inputs vector is represented as $U = [U_1 \quad U_2]^T = [\Delta y_c \quad M_z]^T$. Then, (2) and (3) are written as follows by taking $\beta \cong v_y/v_x$:

$$\dot{\beta} = -r + \frac{1}{mv_x}(F_{yf} + F_{yr}) + \frac{1}{mv_x}\Delta y_c, \tag{25}$$

$$\dot{r} = \frac{1}{I_{zz}}[aF_{yf} - bF_{yr}] + \frac{a}{I_{zz}}\Delta y_c + \frac{1}{I_{zz}}M_z, \tag{26}$$

where F_{yf} and F_{yr} are the lateral forces of the front and rear tires, respectively. M_z is the external yaw moment generated by DYC system as

$$M_z = \frac{T}{2}[(F_{xfL} + F_{xrL}) - (F_{xfR} + F_{xrR})]. \tag{27}$$

Considering the unknown road condition represented by the coefficient (μ) included in the Dugoff model uncertainty depending on the different road conditions, a problem arises in proving stability due to the presence of switching in the Dugoff model calculating the forces of the front and rear side tires, (13). This problem is solved by estimating these forces and using them for feedback. In this work, we can calculate the lateral tire force using the tire slip angle as a second-order polynomial whose slope is equal to the tire stiffness and whose peak value is equal to μF_z [15,27]

$$\hat{F}_y = \begin{cases} C_\alpha \alpha_i - sign(\alpha_i)\dfrac{C_\alpha^2}{4\mu F_z}, & |\alpha_i| < \dfrac{2\mu F_z}{C_\alpha}, \\ \mu F_z, & |\alpha_i| \geq \dfrac{2\mu F_z}{C_\alpha}, \end{cases}$$
$$i = f,\ r. \tag{28}$$

A simplified form of equation (16) is used to calculate the slip angle of the front and rear tires

$$\alpha_f = \delta_f - \beta - \frac{ar}{v_x},\ \alpha_r = -\beta + \frac{br}{v_x}. \tag{29}$$

Remark 1: This paper considers some uncertainties in vehicle parameters to study the effect of structured uncertainties on the robustness of the control system, including the total mass, the tire stiffness, and the moment of inertia.

When designing the controller in the upper layer as a MIMO controller, equations (25) and (26) are as follows:

$$\begin{bmatrix} \dot{\beta} \\ \dot{r} \end{bmatrix} = \begin{bmatrix} f_1(x, \delta_f) \\ f_2(x, \delta_f) \end{bmatrix} + \begin{bmatrix} \frac{1}{mv_x} & 0 \\ \frac{a}{I_{zz}} & \frac{1}{I_{zz}} \end{bmatrix} \begin{bmatrix} U_1 \\ U_2 \end{bmatrix}, \tag{30}$$

where ${}_1(x, \delta_f) = -r + \frac{1}{mv_x}(F_{yf} + F_{yr})$ and $f_2(x, \delta_f) = \frac{1}{I_{zz}}[aF_{yf} - bF_{yr}]$.

The sliding surface vector for tracking the yaw rate and maintaining the slip angle within the stable zone is defined as

$$\begin{bmatrix} S_1 \\ S_2 \end{bmatrix} = \begin{bmatrix} y_1 - y_{1d} \\ y_1 - y_{1d} \end{bmatrix} = \begin{bmatrix} \beta - \beta_d \\ r - r_d \end{bmatrix}. \tag{31}$$

Taking the derivative of (31) and substituting (30) into (32)

$$\begin{bmatrix} \dot{S}_1 \\ \dot{S}_2 \end{bmatrix} = \begin{bmatrix} \dot{\beta} - \dot{\beta}_d \\ \dot{r} - \dot{r}_d \end{bmatrix}$$
$$= \begin{bmatrix} \hat{f}_1(x, \delta_f) - \dot{\beta}_d \\ \hat{f}_2(x, \delta_f) - \dot{r}_d \end{bmatrix} + \begin{bmatrix} \frac{1}{\hat{m}v_x} & 0 \\ \frac{a}{\hat{I}_{zz}} & \frac{1}{\hat{I}_{zz}} \end{bmatrix} \begin{bmatrix} U_1 \\ U_2 \end{bmatrix}. \tag{32}$$

The nonlinear dynamics $f_1(x, \delta_f)$, $f_2(x, \delta_f)$ are not known exactly, but is estimated as $\hat{f}_1(x, \delta_f)$, $\hat{f}_2(x, \delta_f)$, and $\hat{m}$, $\hat{I}_{zz}$ are the parametric uncertainties in the nonlinear dynamics vector and in the control gain matrix.

Making (32) equal to zero, the equivalent control vector is obtained

$$\begin{bmatrix} U_{1eq} \\ U_{2eq} \end{bmatrix} = -inv \begin{bmatrix} \frac{1}{\hat{m}v_x} & 0 \\ \frac{a}{\hat{I}_{zz}} & \frac{1}{\hat{I}_{zz}} \end{bmatrix} \begin{bmatrix} \hat{f}_1(x, \delta_f) - \dot{\beta}_d \\ \hat{f}_2(x, \delta_f) - \dot{r}_d \end{bmatrix}. \tag{33}$$

To ensure the convergence of the sliding variable in finite time, the control input vector based on conventional sliding mode theory is designed as follows:

$$\begin{bmatrix} U_1 \\ U_2 \end{bmatrix} = \begin{bmatrix} \hat{m}v_x & 0 \\ -a\hat{m}v_x & \hat{I}_{zz} \end{bmatrix} \left[\begin{bmatrix} r - \frac{1}{\hat{m}v_x}(F_{yf} + F_{yr}) + \dot{\beta}_d \\ -\frac{1}{\hat{I}_{zz}}[aF_{yf} - bF_{yr}] + \dot{r}_d \end{bmatrix} \right.$$

$$-\begin{bmatrix} K_1 & 0 \\ 0 & K_2 \end{bmatrix}\begin{bmatrix} sign(S_1) \\ sign(S_2) \end{bmatrix}\Bigg]. \quad (34)$$

The MIMO nonlinear system of the vehicle can be expressed to investigate the finite-time stability of the sliding variable as

$$\dot{x} = f(x,t) + g(x,t)u, \\ y = h(x,t), \quad (35)$$

where $x = [x_1 \quad x_2 \quad \ldots \quad x_n]^T$ is the state vector and $y = [y_1 \quad y_2 \quad \ldots \quad y_m]^T$ is the output vector, the coefficients of which are nonlinear functions $h_j(x,t)$, $j = 1, \ldots, m$ and $f(x,t)$ is the n-dimensional vector, the coefficients of which are nonlinear functions $f_i(x,t)$, $i = 1, \ldots, n$, and $g(x,t)$ is a $(n \times p)$ matrix which coefficients are the nonlinear functions $g_{ij}(x,t)$, $i = 1, \ldots, n$ and $j = 1, \ldots, m$ and $u = [u_1 \quad u_2 \quad \ldots \quad u_p]^T$ is the control vector.

Assumption 4: The error estimation and the parametric uncertainties in the nonlinear function and control gains satisfy the following bounds

$$|f_i - \hat{f}_i| \le L_{fi}, \\ |\Delta_{ij}| \le D_{ij}, \ G(x) = (I+\Delta)\hat{G}(x),$$

where

$$G(x) = g_{ij}(x,t) = \begin{bmatrix} g_{11}(x) & \cdots & g_{1j}(x) \\ \vdots & \ddots & \vdots \\ g_{i1}(x) & \cdots & g_{ij}(x) \end{bmatrix}.$$

Lemma 1: Considering the nonlinear MIMO system as (35), the control law (36) leads sliding surfaces (37) go to zero in the finite time and tracking errors asymptotically vanish.

$$U = \hat{G}(x)^{-1}[\zeta_d - \hat{f}(x) - Ksign(S)], \quad (36)$$
$$S = [S_1 \quad \ldots \quad S_p]^T. \quad (37)$$

Proof: Considering a set of sliding surfaces (37) [28].

Assumption 5: In our system, the m-dimensional vector, n-dimensional vector, and p-dimensional control vector are equal. ($m = n = p$), then sliding surfaces become as follows:

$$S_j = \Big(\frac{d}{dt} + \lambda_j\Big)^{r_j - 1} e_j; \ e_j = y_j - y_{jd}, \ j = 1, \ldots, p, \quad (38)$$

where λ_j is a positive scalar, y_{jd} is the desired trajectory, and r_j is the relative degree of the system.

For the vehicle system $r_j = 1$. Then, the set of the sliding surface is

$$S_j = e_j = y_j - y_{jd}. \quad (39)$$

Taking the derivative of equation (37) while putting $\zeta_d = [\dot{y}_{1d} \quad \dot{y}_{2d} \quad \dot{y}_{pd}]^T$ and $\dot{S} = [\dot{S}_1 \quad \dot{S}_2 \quad \dot{S}_p]^T$

$$\dot{S} = f(x) - \zeta_d + G(x)U. \quad (40)$$

The control input vector is designed as (36) in order to ensure the sliding variable's convergence at finite time, where

$$K = \begin{bmatrix} K_{11} & 0 & \cdots & 0 \\ 0 & K_{22} & \cdots & 0 \\ \vdots & 0 & \ddots & 0 \\ 0 & \cdots & \cdots & K_{pp} \end{bmatrix},$$

and

$$sign(S) = [sign(S_1) \ \ sign(S_2) \ \ \ldots \ \ sign(S_p)]^T.$$

By utilizing the controller (36) in conjunction with the system (40)

$$\dot{S} = f(x) - \zeta_d \\ + (I+\Delta)\hat{G}(x)\hat{G}(x)^{-1}[\zeta_d - \hat{f}(x) - Ksign(S)].$$

Using some algebraic operations on the previous equation yields

$$\dot{S} = f(x) - \hat{f}(x) + \Delta(\zeta_d - \hat{f}(x)) - (I+\Delta)Ksign(S). \quad (41)$$

The following positive definite Lyapunov function can be used to investigate sliding variables' stability in finite time [28]

$$V_j(S,t) = \frac{1}{2}S_j^T S_j, \ j = 1, \ldots, p. \quad (42)$$

The following condition is taken into consideration to guarantee the sliding variables' finite-time convergence

$$\dot{V}_j(S,t) = \frac{\partial V_j(S,t)}{\partial S_j} = S_j^T \dot{S}_j \le -\eta_j |S_j|, \quad (43)$$

where η_j is a positive constant.

Substituting (41) into (43),

$$\frac{S_j^T}{|S_j|}\big[(f_j(x) - \hat{f}_j(x)) + \Delta_{ij}(\zeta_{dj} - \hat{f}_j(x)) \\ - (I+\Delta_{ij})K_{jj}sign(S_j)\big] \le -\eta_j, \\ \frac{S_j^T}{|S_j|}(f_j(x) - \hat{f}_j(x)) + \frac{S_j^T}{|S_j|}\Delta_{ij}(\zeta_{dj} - \hat{f}_j(x)) \\ - (I+\Delta_{ij})K_{jj} \le -\eta_j.$$

Choosing the maximum values of estimate errors and the parametric uncertainties yields

$$L_{fj} + D_{ij}\left|\zeta_{dj} - \hat{f}_j(x)\right| - (I+D_{ij})K_{jj} \le -\eta_j. \quad (44)$$

As a result, the sliding condition is confirmed when

$$K_{jj} > L_{fj} + D_{ij}\left|\zeta_{dj} - \hat{f}_j(x)\right|.$$

Consequently, using the controller (36) to control the system (40) ensures that the sliding variables will eventually reach zero and tracking errors asymptotically vanish.

Lemma 2: Considering the nonlinear MIMO system (35) and the first derivative of uncertainties estimation (45) as the form of the observer (28), the control law (36) leads sliding surfaces (37) to go to zero in the finite time and tracking errors asymptotically vanish.

$$\dot{\hat{f}}_J(x) = \Gamma_j sign(\alpha_i);\ i = f,\ r. \tag{45}$$

Proof: To investigate the finite-time stability of a closed-loop system, the Lyapunov is considered as

$$V_j(S,t) = \frac{1}{2}S_j^T S_j + \frac{1}{2}(f_j(x) - \hat{f}_j(x))^T (f_j(x) - \hat{f}_j(x)),\\ j = 1,\ ...,\ p. \tag{46}$$

The following condition is taken into account to ensure the sliding variables' finite-time convergence

$$\begin{aligned}\dot{V}_j(S,t) = {} & \frac{\partial V_j(S,t)}{\partial S_j} \\ & = S_j^T \dot{S}_j + (f_j(x) - \hat{f}_j(x))^T (\dot{f}_j(x) - \dot{\hat{f}}_J(x)) \\ & \le -\eta_j |S_j|. \end{aligned} \tag{47}$$

Substituting (41) and (45) into (47)

$$\begin{aligned} & \frac{S_j^T}{|S_j|}[(f_j(x) - \hat{f}_j(x)) + \Delta_{ij}(\zeta_{d\,j} - \hat{f}_j(x)) \\ & \quad - (I + \Delta_{ij} K_{jj} sign(S_j)] \\ & \quad + (f_j(x) - \hat{f}_j(x))^T (\dot{f}_j(x) - \dot{\hat{f}}_J(x)) \le -\eta_j, \\ & \frac{S_j^T}{|S_j|}(f_j(x) - \hat{f}_j(x)) + \frac{S_j^T}{|S_j|}\Delta_{ij}(\zeta_{d\,j} - \hat{f}_j(x)) \\ & \quad - \frac{S_j^T}{|S_j|}(I + \Delta_{ij})K_{jj} sign(S_j) \\ & \quad + \frac{S_j^T}{|S_j|}(f_j(x) - \hat{f}_j(x))^T (\dot{f}_j(x) - \Gamma_j sign(\alpha_i)) \le -\eta_j. \end{aligned}$$

Assumption 6: The first derivative of uncertainties estimation $\dot{f}_j(x)$ is bounded by some known function $L_{\dot{f}\,j}$.

Based on Assumption 6, the following result is obtained

$$\begin{aligned} & L_{f\,j} + D_{ij}\left|\zeta_{d\,j} - \hat{f}_j(x)\right| - (I + D_{ij})Kjj + L_{f\,j}^T L_{\dot{f}\,j} \\ & \quad - L_{f\,j}^T \Gamma_j \le -\eta_j. \end{aligned} \tag{48}$$

Therefore, the control law (36) leads sliding surfaces (37) to go to zero in the finite time and tracking errors asymptotically vanish when

$$K_{jj} > L_{f\,j} + D_{ij}\left|\zeta_{d\,j} - \hat{f}_j(x)\right| + L_{f\,j}^T L_{\dot{f}\,j}.$$

The chattering caused by the function (sign) is eliminated in several ways, including observer-based slip mode [29], adaptive sliding mode [30], and higher-order sliding mode [31]. A tangent hyperbolic approach is presented in [32] and used in this article. Therefore, the control laws of the upper control layer are defined as

$$\begin{aligned}\begin{bmatrix} U_1 \\ U_2 \end{bmatrix} = \begin{bmatrix} \hat{m}v_x & 0 \\ -a\hat{m}v_x & \hat{I}_{zz} \end{bmatrix} & \left[\begin{bmatrix} r - \frac{1}{\hat{m}v_x}(F_{yf} + F_{yr}) + \dot{\beta}_d \\ -\frac{1}{\hat{I}_{zz}}[aF_{yf} - bF_{yr}] + \dot{r}_d \end{bmatrix}\right. \\ & \left. - \begin{bmatrix} K_1 & 0 \\ 0 & K_2 \end{bmatrix} \begin{bmatrix} \tanh(S_1/\varphi_1) \\ \tanh(S_1/\varphi_1) \end{bmatrix}\right], \end{aligned} \tag{49}$$

where $\varphi_i > 0$; $i = 1, 2$ is the design parameter indicating the boundary layer range about the sliding surface.

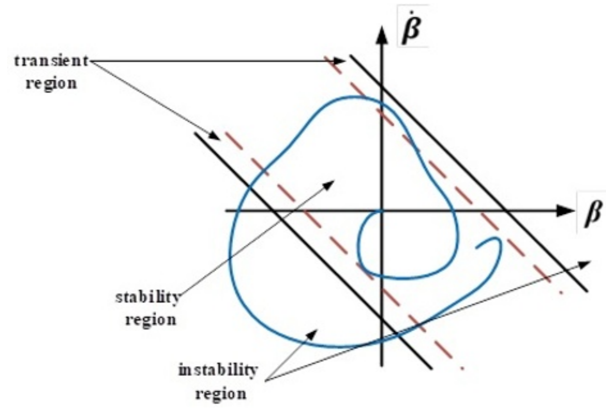

Fig. 7. Division regions in the $\beta - \dot{\beta}$ phase plane.

3.2. Coordination of AFS and DYC

As part of the integrated vehicle dynamics control strategy, the AFS system can control the yaw rate in the handling region. The DYC system is activated when the vehicle's handling capabilities are exceeded. For this purpose, the vehicle's stability is described in this section using the $\beta - \dot{\beta}$ phase plane, which is the phase plane of the vehicle sideslip angle and its time derivative [7,19,33]. The stability index χ is defined as follows for determining the stability region [19]:

$$\chi = \left|2.4979\dot{\beta} + 9.549\beta\right|,\ \chi < 1. \tag{50}$$

Equation (50) divides the vehicle's phase plane into stability, transient, and instability regions, as shown in Fig. 7. When the vehicle enters the stable area, only the AFS system controls its handling. Once the car reaches the transient region due to various reasons related to sudden changes in the path and the tire's coefficient of road friction, the DYC system is engaged to generate additional torque to bring the vehicle back to the stable region. The pure DYC system is activated when the vehicle enters an instability region to force the vehicle to return to the stable region. This is done because of the yaw moment's insensitivity to the compensating steering angle generated by the AFS as a result of tire saturation.

The adaptation gain $\rho(\chi)$ is defined as follows to control the two systems (DYC and AFS):

$$\rho(\chi) = \begin{cases} 0, & \chi \leq 0.8, \quad \text{Only AFS}, \\ -5SI+5, & 0.8 < \chi \leq 1, \quad \text{AFS+DYC}, \\ 1, & \chi > 1, \quad \text{Only DYC}. \end{cases} \tag{51}$$

3.3. Low level controller design

In this layer, the corrective yaw moment M_z resulting from the first control law in the upper layer is converted to the braking torque of the rear tires using a wheel slip controller to avoid saturation of the tire forces caused by M_z in the upper layer. The desired longitudinal forces for the rear tires are calculated through (52) and substituted into the Dugof Model to produce the desired longitudinal slip ratio (λ_d).

$$M_z = T\Delta F_x/2. \tag{52}$$

The wheel slip controller is designed to generate the final distributed braking torque for producing the longitudinal forces required for the rear tires in order to achieve the corrective yaw moment.

3.3.1 Wheel slip controller design

Non-linearity and uncertainty are the main challenges when designing a wheel slip controller. For this type of problem, SMC is a suitable approach due to its robustness [34,35].

A sliding surface S_3 is defined as

$$S_3 = \lambda - \lambda_d. \tag{53}$$

Taking the derivative of the sliding surface

$$\dot{S}_3 = \dot{\lambda} - \dot{\lambda}_d. \tag{54}$$

Taking the time derivative from (15) where $(-1 < \lambda < 0)$

$$\dot{\lambda}_i = \frac{1}{v_{xwi}}[R_w\dot{\omega}_i - \frac{R_w\omega_i}{v_{xwi}}\dot{v}_{xwi}], \; i = rL, \; rR. \tag{55}$$

By substituting (5) and (15) into (55), $\dot{\lambda}_i$ is obtained

$$\dot{\lambda}_i = \frac{(1+\lambda_i)}{I_w\omega_i}\left(R_wF_{ti} + \frac{I_w(1+\lambda_i)}{R_w}\dot{v}_{xwi}\right) + \frac{(1+\lambda_i)}{I_w\omega_i}T_{bi}, \; i = rL, \; rR. \tag{56}$$

Taking the time derivative of (15) where $(0 < \lambda < 1)$

$$\dot{\lambda}_i = \frac{1}{\omega_i}\left[-\frac{\dot{v}_{xwi}}{R_w} + \frac{v_{xwi}\dot{\omega}_i}{R_w\omega_i}\right], \; i = rL, \; rR. \tag{57}$$

$\dot{\lambda}_i$ can be obtained by incorporating (5) and (15) into (57)

$$\dot{\lambda}_i = -\frac{(1+\lambda_i)}{I_w\omega_i}\left(R_wF_{ti} + \frac{I_w}{(1-\lambda_i)R_w}\dot{v}_{xwi}\right) + \frac{(1-\lambda_i)}{I_w\omega_i}T_{bi}, \; i = rL, \; rR. \tag{58}$$

The longitudinal wheel acceleration $(\dot{v}_{xwi})$ is not defined in (56) and (58). It is estimated either by constraining it to an upper bound using the sliding mode control properties in the presence of uncertainties [35] or by approximating the longitudinal acceleration (a_x) of the vehicle [15]. The second method was used in this work to estimate the longitudinal wheel acceleration. Furthermore, the observer must estimate the longitudinal forces since they cannot be measured directly [36]. To include the two cases of λ in (56) and (58), $\dot{\lambda}_i$ can be written as follows:

$$\dot{\lambda}_i = -\frac{(1-|\lambda_i|)}{I_w\omega_i}\left(R_w\hat{F}_{ti} + \frac{I_w}{R_w}a_x\right) + \frac{(1-|\lambda_i|)}{I_w\omega_i}T_{bi}, \; i = rL, \; rR. \tag{59}$$

The equivalent braking torque is calculated by substituting (59) into (54) and setting it equal to zero

$$T_{bieq} = \frac{I_w\omega_i}{(1-|\lambda_i|)}[\frac{(1-|\lambda_i|)}{I_w\omega_i}(R_w\hat{F}_{ti} + \frac{I_w}{R_w}a_x) + \dot{\lambda}_{di}], \; i = rL, \; rR. \tag{60}$$

The total control law, which uses the tangent hyperbolic function, is presented in [37]

$$T_{bi} = R_w\hat{F}_{ti} + \frac{I_w}{R_w}a_x + \frac{I_w\omega_i}{(1-|\lambda_i|)}(\dot{\lambda}_{di} - K_3\tanh(S_3/\varphi_3)), \; i = rL, \; rR, \tag{61}$$

where $\varphi_3 > 0$.

According to Lyapunov stability [28], K_3 can be calculated as

$$K_3 \geq F + \eta_3, \tag{62}$$

where η_3 is a positive constant.

4. SIMULATION RESULTS AND DISCUSSION

A simulation of the 8-DoF model of the vehicle and the proposed control system were conducted using MATLAB/Simulink software to evaluate the vehicle performance with the proposed integrated vehicle dynamics control (IVDC) algorithm combined with active front steering and differential braking systems. Several parameters associated with the vehicle model for the controlling system

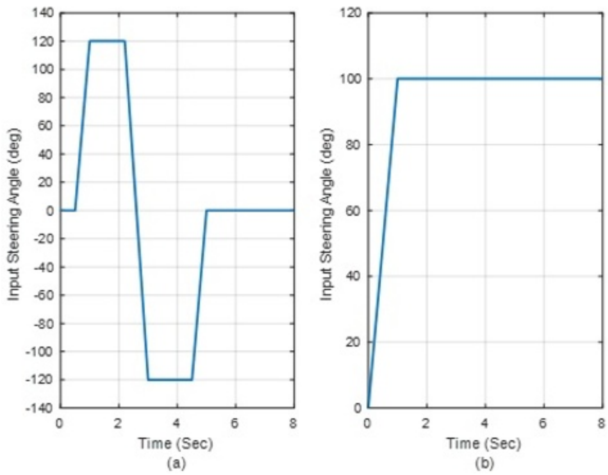

Fig. 8. Wheel steering angle: (a) Double lane-change maneuver and (b) J-turn maneuver.

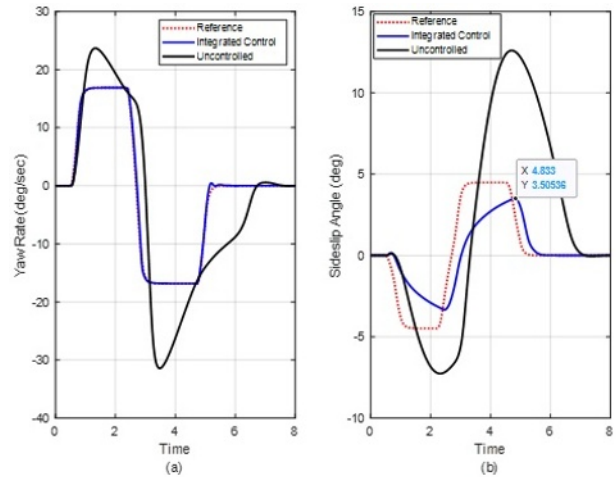

Fig. 9. Response of the vehicle to a double lane-change manoeuvre on gravel road ($\mu = 0.6$): (a) Yaw rate (deg/s) and (b) sideslip angle (deg).

are listed in Table 1. Different scenarios are presented in this section to analyze the effects of the proposed control strategies on lateral vehicle stability and investigate the proposed controllers' robustness to tire-road friction coefficient and steer angle variations. Therefore, there are two different road conditions and two different maneuvers (Double lane change and J-turn), as shown in Fig. 8. The vehicle parameter uncertainties can be considered as +10% in the vehicle mass, +15% in the moment of inertia, and -15% in the tire stiffness. Simulation results include the yaw rate, side slip angle, lateral acceleration, braking torque, and corrective yaw moment. This paper considers the ratio between the angles turned by the steering wheel and the road wheel to be 20.

4.1. Gravel road double lane-change maneuver

The tire-road friction coefficient (μ) for carvel roads is set to 0.6. In this maneuver, comparing the proposed controller performance at a longitudinal velocity of 20 m/s, the proposed controller robustness and effectiveness to the input steering angle variations are validated. Fig. 9 shows the yaw rate and slip angle effect on the vehicle's response. In a controlled vehicle, the yaw rate would always follow the desired value. In an uncontrolled vehicle, the yaw rate would always be greater than the desired value, resulting in instability. During the whole maneuver, the sideslip angle for the controlled vehicle remains within the upper and lower bounds, while uncontrolled vehicles' sideslip angles increase significantly, resulting in vehicle instability.

Increasing the yaw rate and sideslip angle for uncontrolled vehicles lead to high lateral acceleration. Fig. 10(a) shows how lateral acceleration differs between controlled and uncontrolled vehicles. Fig. 10(b) shows how well the actual lateral forces of the tires match the estimated ones.

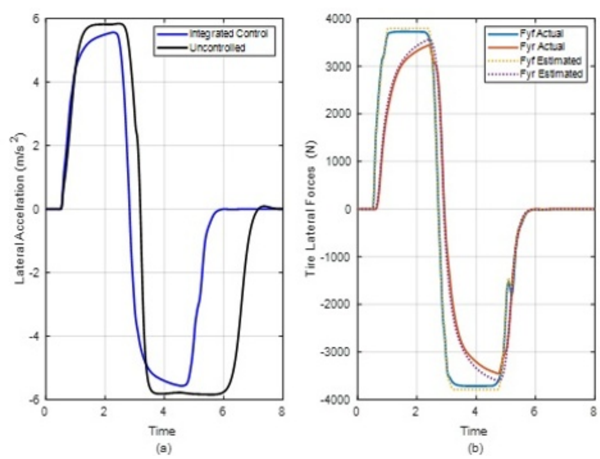

Fig. 10. An evaluation of the lateral acceleration and lateral forces for ($\mu = 0.6$) by considering double lane-change maneuver: (a) The lateral acceleration and (b) the lateral forces of the tires.

Fig. 11 shows how the stability index and work zones of the (DYC and AFS) systems evolve according to changing driving conditions. Based on (51) and Fig. 11, when the stability index satisfies $\chi \leq 0.8$, only AFS improves the handling performances. However, when $0.8 < \chi \leq 1$, the DYC system and AFS work together to maintain vehicle stability. The pure DYC system is activated when $\chi > 1$, bringing the vehicle back to the safe zone. Fig. 12 shows the phase-plane diagram of dynamic sideslip angle changes. The trajectory of the controlled vehicle in the phase plane leaves the stable region to be immediately drawn into this area due to the brake system intervention. Figs. 13(a) and 13(b) illustrate the right and left brake torques generated by the corrective yaw moment at the lower control level. Fig. 14 also shows the external

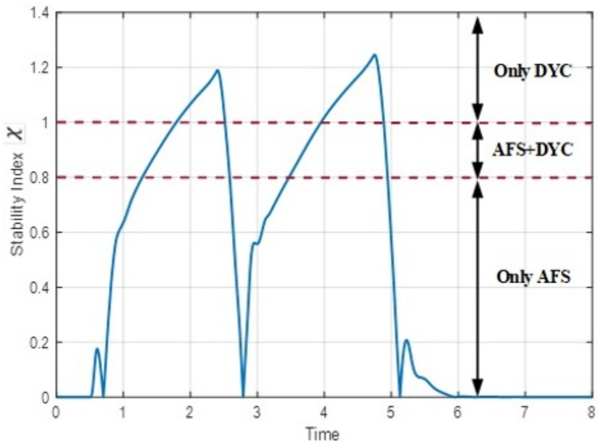

Fig. 11. Stability index vs. time for ($\mu = 0.6$) by considering double lane-change maneuver.

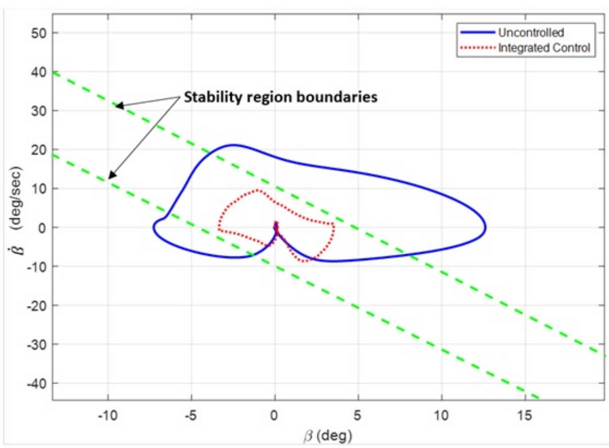

Fig. 12. Phase plane stability evaluation for the double-lane-change maneuver on a gravel road.

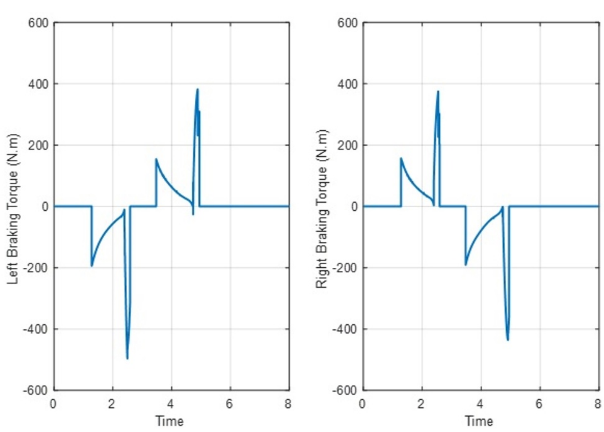

Fig. 13. An evaluation of braking torques with integrated control for ($\mu = 0.6$): (a) Rear-left braking torque and (b) rear-right braking torque.

yaw moment and the amount of corrective steering angle for the wheels participating in the integrated system.

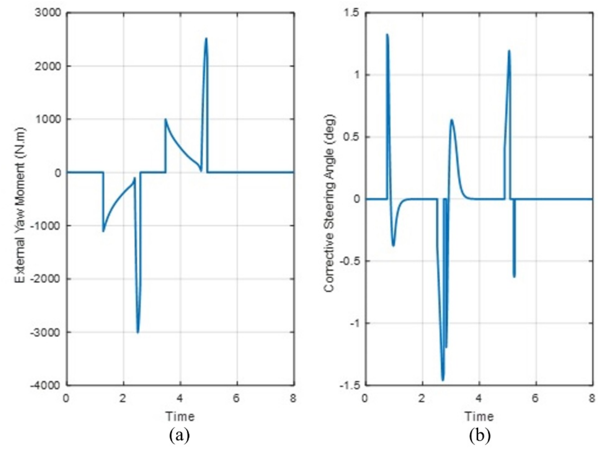

Fig. 14. An evaluation of the corrective yaw moment and compensatory steering angle for integrated control on a gravel road ($\mu = 0.6$) by considering double lane-change maneuver: (a) The external yaw moment. (b) Corrective steering angle.

4.2. J-turn maneuver on a slippery road

In this maneuver, the vehicle runs on a slippery road at 80 km/h with $\mu = 0.4$. In terms of the vehicle's response in the J-turn maneuver, one of the objectives of this paper is to compare the integrated sliding mode controller to the integrated adaptive controller introduced in [12].

Fig. 15(a) depicts the tracking performance of the yaw rate of both MSMC and MAC are nearly close to the reference yaw rate. However, in the uncontrolled case, a considerable yaw rate tracking error can be seen. In addition, in the sense of vehicle handling and stability, the sideslip angles of both MSMC and MAC controllers have decreased as compared to the uncontrolled vehicle, which indicates limiting in lateral slip using both mentioned con-

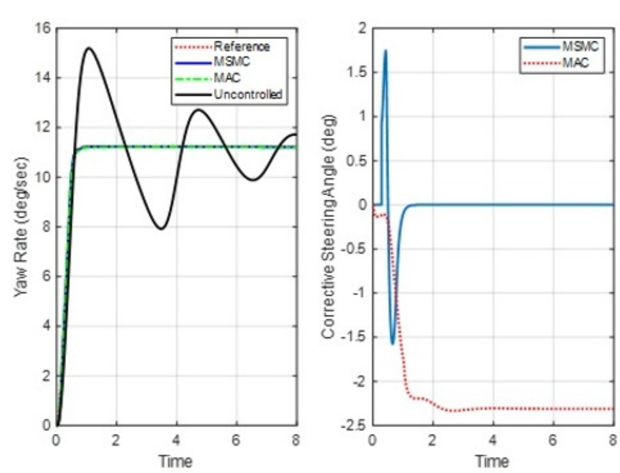

Fig. 15. An evaluation of the corrective yaw moment and compensatory steering angle on a slippery road during the J-turn maneuver.

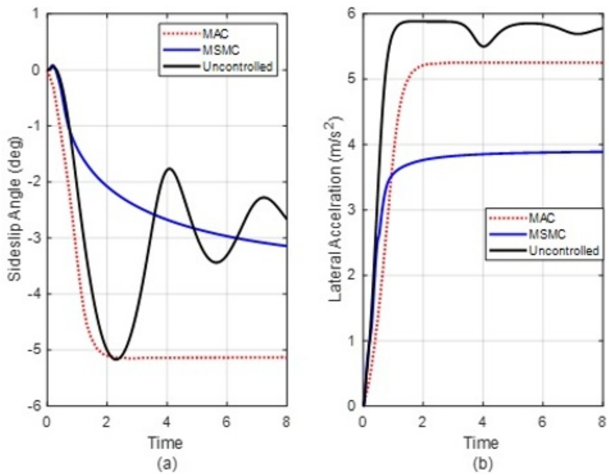

Fig. 16. Comparison of the lateral slip angle and lateral acceleration for the J-turn maneuver on a slippery road ($\mu = 0.4$).

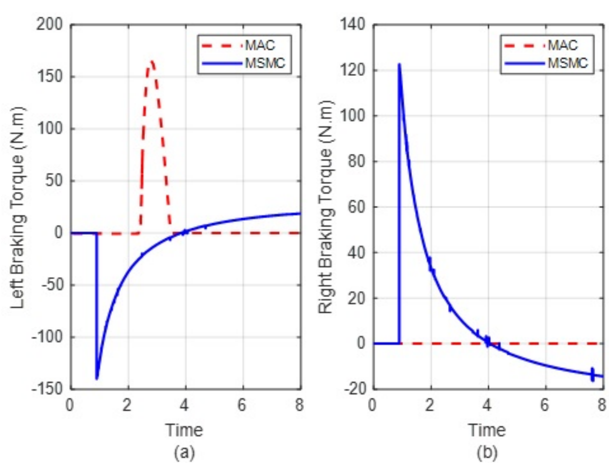

Fig. 17. Comparison of braking torques for the J-turn maneuver on a slippery road ($\mu = 0.4$): (a) Left braking torque ($N.m$) and (b) right braking torque ($N.m$).

trollers. According to Figs. 15(b) and 17, MSMC can produce a good tracking performance by spending less additive steering angle but extra control effort as compared to MAC.

Figs. 16(a) and 16(b) show that the lateral slip angle and lateral acceleration are less than the uncontrolled case; however, sliding mode controller achieves lower peaks for the lateral acceleration in response to the steering input and guarantees less slip but in the expense of a longer application time of the braking torque as shown in Fig. 17.

Fig. 18 depicts the alterations in sideslip dynamics within the phase plane diagram. As demonstrated in Fig. 14, two control scenarios can ensure that the vehicle remains within the stable region and does not transition into the unstable region. This is due to the decreased lateral acceleration and sideslip angles of both MSMC and MAC controllers relative to the uncontrolled vehicle. The MSMC method, which employs a coordination algorithm between AFS and DYC of the current research, effectively maintains lateral vehicle dynamics within the stable region compared to the MAC method, albeit at the expense of an increase in the duration of braking torque applied to the rear wheels. Tracking performance is improved due to reduced lateral sideslip angle and lateral acceleration, as shown in Fig. 16.

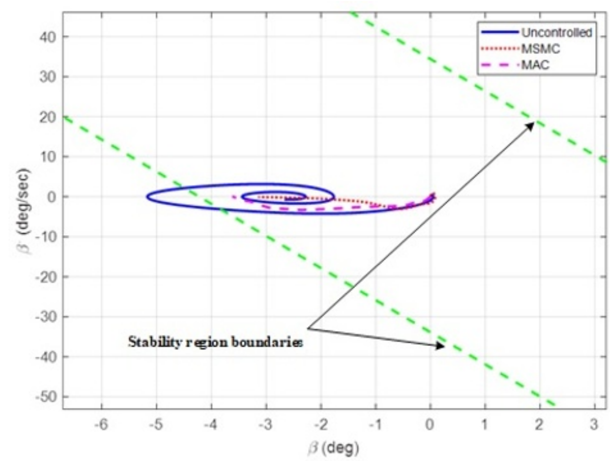

Fig. 18. Phase plane stability evaluation for the J-turn maneuver on a slippery road.

As a result of the proposed control algorithm, yaw stability control can be achieved with increased braking torque applied to the rear wheels compared to the adaptive method.

4.3. J-turn maneuver for sudden entry onto a slippery road

The vehicle performs this maneuver at 80 km/h on a dry road with a 0.9 adhesion coefficient. An 80° steering wheel angle input initiates a J-turn, and after two seconds, the vehicle abruptly enters a section of an icy road with a coefficient of adhesion of 0.2. This section aims to ensure that the proposed control system can be robust against steering angles and road conditions changes.

The uncontrolled vehicle has yaw rate oscillation. Its sideslip angle increases as soon as it enters the ice-covered road, as depicted in Figs. 19(a) and 19(b), making the vehicle unstable. The vehicle's yaw rate and sideslip angle reach acceptable levels in the controlled case, allowing for steady responses, as shown in Figs. 19(a) and 19(b). AFS and DYC produce the corrective yaw moment into stability, transient and instability regions. Figs. 20(a) and 20(b) also show the external yaw moment and the amount of corrective steering angle for the wheels involved in the integrated system to keep the vehicle within the stable area, as shown in Fig. 21.

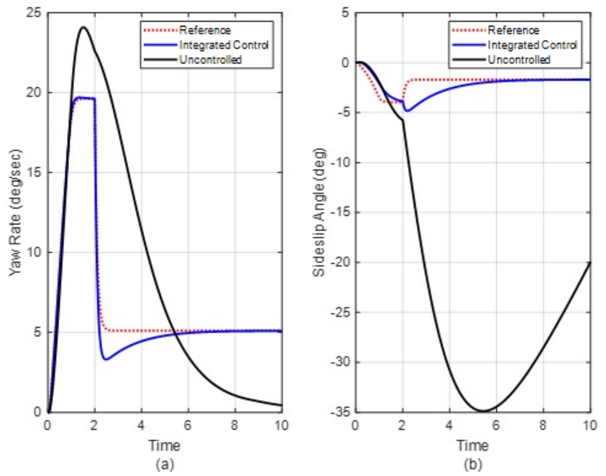

Fig. 19. J-turn manoeuvre response of vehicle for a sudden entry onto a slippery road: (a) Yaw rate (deg/s) and (b) sideslip angle (deg).

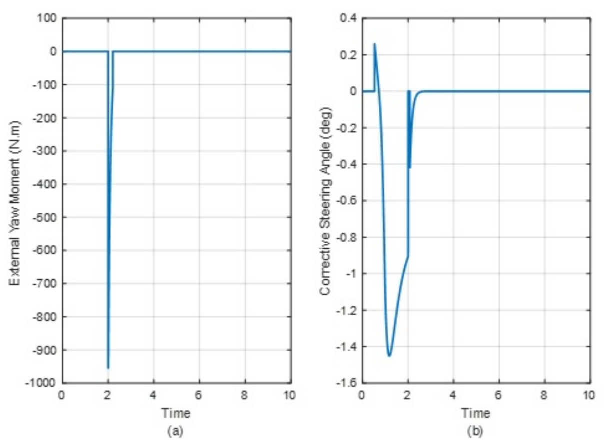

Fig. 20. J-turn manoeuvre response of vehicle for a sudden entry onto a slippery road: (a) Yaw rate (deg/s) and (b) sideslip angle (deg).

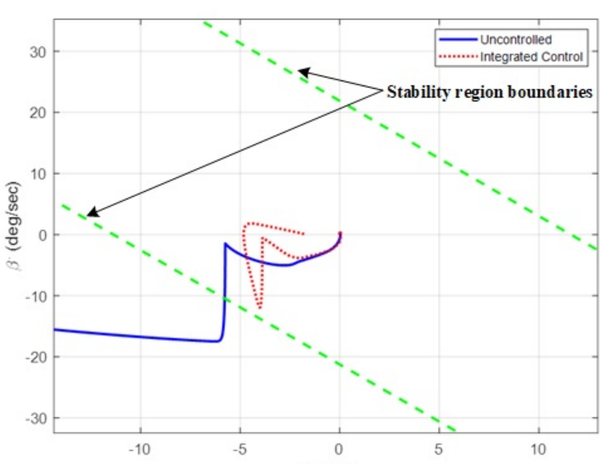

Fig. 21. Phase plane stability evaluation for the J-turn maneuver for a sudden entry onto a slippery road.

5. CONCLUSION

The main objective of this work is to improve vehicle stability in critical driving situations. A hierarchical control strategy based on sliding mode control developed the coordination between AFS and DYC via adaption gain. The proposed control structure consists of two layers. The main objective of the upper layer is to generate an accurate external yaw moment and corrective front steering angle based on the MIMO Sliding Mode controller. The slip controller in the lower layer based on SMC generates the final distributed braking torques. The efficacy of the proposed method was evaluated by simulating two scenarios in various road conditions using a nonlinear 8-DOF vehicle model to ensure that the proposed control system is robust against road condition changes. The simulation results compared the suggested sliding mode integrated controller's efficiency to that of an adaptive integrated controller [12]. The results showed that the proposed control system tracked the desired yaw rate and kept the sideslip angle equal to or less than the desired value with fewer control efforts. The most significant disadvantage of the proposed control method is that the discontinuous function gain needs to be determined in such a way as to overcome the uncertainties present in the system. To select a suitable discontinuous function gain, we need to know the upper bound of uncertainties, the variation of parameters, etc. Therefore, in future studies, the adaptive MIMO sliding mode control (AMSMC) will be designed by replacing the discontinuous function gain with a time-varying parameter to solve the problem of not knowing the upper bound of uncertainties.

CONFLICT OF INTEREST

The authors declare that there is no competing financial interest or personal relationship that could have appeared to influence the work reported in this paper.

REFERENCES

[1] F. Yu, D.-F. Li, and D. Crolla, "Integrated vehicle dynamics control—state-of-the art review," *Proc. of IEEE Vehicle Power and Propulsion Conference*, IEEE, pp. 1-6, 2008.

[2] doiA. Goodarzi and M. Alirezaie, "Integrated fuzzy/optimal vehicle dynamic control," *International Journal of Automotive Technology*, vol. 10, no. 5, pp. 567-575, 2009.10.1007/s12239-009-0066-5

[3] J. Zhao, P. K. Wong, X. Ma, and Z. Xie, "Chassis integrated control for active suspension, active front steering and direct yaw moment systems using hierarchical strategy," *Vehicle System Dynamics*, vol. 55, no. 1, pp. 72-103, 2017.

[4] B. Li, S. Rakheja, and Y. Feng, "Enhancement of vehicle stability through integration of direct yaw moment and

active rear steering," *Proc. of the Institution of Mechanical Engineers, Part D: Journal of Automobile Engineering*, vol. 230, no. 6, pp. 830-840, 2016.

[5] J. He, D. A. Crolla, M. Levesley, and W. Manning, "Coordination of active steering, driveline, and braking for integrated vehicle dynamics control," *Proc. of the Institution of Mechanical Engineers, Part D: Journal of Automobile Engineering*, vol. 220, no. 10, pp. 1401-1420, 2006.

[6] S. Cheng, L. Li, H.-Q. Guo, Z.-G. Chen, and P. Song, "Longitudinal collision avoidance and lateral stability adaptive control system based on MPC of autonomous vehicles," *IEEE Transactions on Intelligent Transportation Systems*, vol. 21, no. 6, pp. 2376-2385, 2019.

[7] N. Ahmadian, A. Khosravi, and P. Sarhadi, "Integrated model reference adaptive control to coordinate active front steering and direct yaw moment control," *ISA Transactions*, vol. 106, pp. 85-96, 2020.

[8] H. Mirzaeinejad, M. Mirzaei, and S. Rafatnia, "A novel technique for optimal integration of active steering and differential braking with estimation to improve vehicle directional stability," *ISA Transactions*, vol. 80, pp. 513-527, 2018.

[9] M. Jalali, S. Khosravani, A. Khajepour, S.-K. Chen, and B. Litkouhi, "Model predictive control of vehicle stability using coordinated active steering and differential brakes," *Mechatronics*, vol. 48, pp. 30-41, 2017.

[10] M. Doumiati, O. Sename, L. Dugard, J.-J. Martinez-Molina, P. Gaspar, and Z. Szabo, "Integrated vehicle dynamics control via coordination of active front steering and rear braking," *European Journal of Control*, vol. 19, no. 2, pp. 121-143, 2013.

[11] M. Mirzaei and H. Mirzaeinejad, "Fuzzy scheduled optimal control of integrated vehicle braking and steering systems," *IEEE/ASME Transactions on Mechatronics*, vol. 22, no. 5, pp. 2369-2379, 2017.

[12] N. Ahmadian, A. Khosravi, and P. Sarhadi, "Driver assistant yaw stability control via integration of AFS and DYC," *Vehicle System Dynamics*, vol. 60, no. 5, pp. 1742-1762, 2022.

[13] N. Ding and S. Taheri, "An adaptive integrated algorithm for active front steering and direct yaw moment control based on direct Lyapunov method," *Vehicle System Dynamics*, vol. 48, no. 10, pp. 1193-1213, 2010.

[14] J. Zhang, S. Zhou, F. Li, and J. Zhao, "Integrated nonlinear robust adaptive control for active front steering and direct yaw moment control systems with uncertainty observer," *Transactions of the Institute of Measurement and Control*, vol. 42, no. 16, pp. 3267-3280, 2020.

[15] B. Mashadi and M. Majidi, "Integrated AFS/DYC sliding mode controller for a hybrid electric vehicle," *International Journal of Vehicle Design*, vol. 56, no. 1-4, pp. 246-269, 2011.

[16] A. Saikia and C. Mahanta, "Vehicle stability enhancement using sliding mode based active front steering and direct yaw moment control," *Proc. of Indian Control Conference (ICC)*, IEEE, pp. 378-384, 2017.

[17] J. Feng, S. Chen, and Z. Qi, "Coordinated chassis control of 4WD vehicles utilizing differential braking, traction distribution and active front steering," *IEEE Access*, vol. 8, pp. 81055-81068, 2020.

[18] J. Liu, L. Gao, J. Zhang, and F. Yan, "Super-twisting algorithm second-order sliding mode control for collision avoidance system based on active front steering and direct yaw moment control," *Proc. of the Institution of Mechanical Engineers, Part D: Journal of Automobile Engineering*, vol. 235, no. 1, pp. 43-54, 2021.

[19] J. Zhang and J. Li, "Integrated vehicle chassis control for active front steering and direct yaw moment control based on hierarchical structure," *Transactions of the Institute of Measurement and Control*, vol. 41, no. 9, pp. 2428-2440, 2019.

[20] B. Boada, M. Boada, and V. Diaz, "Fuzzy-logic applied to yaw moment control for vehicle stability," *Vehicle System Dynamics*, vol. 43, no. 10, pp. 753-770, 2005.

[21] D. E. Smith and J. M. Starkey, "Effects of model complexity on the performance of automated vehicle steering controllers: Model development, validation and comparison," *Vehicle System Dynamics*, vol. 24, no. 2, pp. 163-181, 1995.

[22] J. Ni, J. Hu, and C. Xiang, "Envelope control for four-wheel independently actuated autonomous ground vehicle through AFS/DYC integrated control," *IEEE Transactions on Vehicular Technology*, vol. 66, no. 11, pp. 9712-9726, 2017.

[23] R. Rajamani, *Vehicle Dynamics and Control*, Springer Science & Business Media, 2011.

[24] A. N. Asiabar and R. Kazemi, "A direct yaw moment controller for a four in-wheel motor drive electric vehicle using adaptive sliding mode control," *Proc. of the Institution of Mechanical Engineers, Part K: Journal of Multi-body Dynamics*, vol. 233, no. 3, pp. 549-567, 2019.

[25] G. J. Heydinger, W. R. Garrott, and J. P. Chrstos, "The importance of tire lag on simulated transient vehicle response," *SAE Transactions*, pp. 362-374, 1991.

[26] D. Piyabongkarn, R. Rajamani, J. A. Grogg, and J. Y. Lew, "Development and experimental evaluation of a slip angle estimator for vehicle stability control," *IEEE Transactions on Control Systems Technology*, vol. 17, no. 1, pp. 78-88, 2008.

[27] O. Mokhiamar and M. Abe, "Simultaneous optimal distribution of lateral and longitudinal tire forces for the model following control," *Journal of Dynamic Systems, Measurement and Control*, vol. 126, no. 4, pp. 753-763, 2004.

[28] J.-J. E. Slotine and W. Li, *Applied Nonlinear Control*, no. 1, Prentice hall, Englewood Cliffs, NJ, 1991.

[29] V. Behnamgol, A. Vali, and A. Mohammadi, "A new observer-based chattering-free sliding mode guidance law," *Proc. of the Institution of Mechanical Engineers, Part G: Journal of Aerospace Engineering*, vol. 230, no. 8, pp. 1486-1495, 2016.

[30] K. Shao, J. Zheng, C. Yang, F. Xu, X. Wang, and X. Li, "Chattering-free adaptive sliding-mode control of nonlinear systems with unknown disturbances," *Computers & Electrical Engineering*, vol. 96, 107538, 2021.

[31] G. P. Incremona, M. Rubagotti, M. Tanelli, and A. Ferrara, "A general framework for switched and variable gain higher order sliding mode control," *IEEE Transactions on Automatic Control*, vol. 66, no. 4, pp. 1718-1724, 2020.

[32] M. Mancini, E. Capello, and E. Punta, "Sliding mode control with chattering attenuation and hardware constraints in spacecraft applications," *IFAC-PapersOnLine*, vol. 53, no. 2, pp. 5147-5152, 2020.

[33] Y. Liang, Y. Li, Y. Yu, and L. Zheng, "Integrated lateral control for 4WID/4WIS vehicle in high-speed condition considering the magnitude of steering," *Vehicle System Dynamics*, vol. 58, no. 11, pp. 1711-1735, 2020.

[34] A. E. Hadri, J.-C. Cadiou, K.-N. M'Sirdi, and Y. Delanne, "Wheel-slip regulation based on sliding mode approach," *SAE Transactions*, pp. 608-616, 2001.

[35] K. R. Buckholtz, "Reference input wheel slip tracking using sliding mode control," *Sae Transactions*, pp. 477-483, 2002.

[36] M. Tanelli, L. Piroddi, and S. M. Savaresi, "Real-time identification of tire–road friction conditions," *IET Control Theory & Applications*, vol. 3, no. 7, pp. 891-906, 2009.

[37] M. A. A. Semnani, A. Vali, S. Hakimi, and V. Behnamgol, "Modelling and design of observer based smooth sliding mode controller for heart rhythm regulation," *International Journal of Dynamics and Control*, vol. 10, no. 3, pp. 828-842, 2022.

Ebrahim Muhammad received his B.Sc. degree in electronic engineering from Aleppo University, Aleppo, Syria, in 2000, and an M.Sc. degree in control engineering from Malek Ashtar University, Tehran, Iran, in 2010. He currently is a Ph.D. student of control engineering. His current research interests include nonlinear control, sliding mode, and robust control.

Ahmad Reza Vali was born in Iran in 1972. He received his B.Sc. degree in electrical-electronics engineering from the Shiraz University, Shiraz, Iran in 1995 and his M.Sc. and Ph.D. degrees in electrical-control engineering from the Department of Electrical Engineering, Amirkabir University of Technology, Tehran, Iran, in 1998 and 2005, respectively. He is the author of more than 190 Journal and Conference Papers in the field of nonlinear control systems, analysis and control of delay-time systems, tracking systems, modeling and control of biological systems and robotics. Dr. Ahmad Reza Vali is currently an Associate Professor at the Department of Electrical and Computer Engineering, Malek-Ashtar University and Technology, Tehran, Iran.

Abdorreza Kashaninia received his B.S. degree in electrical engineering from University of Tehran in 2001 and his M.S. and Ph.D. degrees from Amirkabir University of Technology, Tehran, Iran, in 2003 and 2011, respectively. From 2012, he is an assistant professor with the Department of Electrical Engineering, Malekashtar University of Technology, Tehran, Iran. His research interests include nonlinear and adaptive control, optimal and predictive control, multiagent systems, and fault tolerant control.

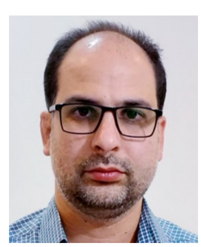

Vahid Behnamgol was born in Iran in 1985. He received his B.S. degree in electrical engineering from Shomal University, Iran, in 2009, and his M.S. and Ph.D. degrees in control engineering from Malek Ashtar University, Tehran, Iran, in 2011 and 2016, respectively. He is currently an assistant professor of the Department of Control, the Malek Ashtar University of Technology of Tehran, Iran. He has authored more than 50 scientific journal and conference papers. His research interests include nonlinear, sliding mode, and robust control and guidance systems.